

Evidence of impact shock metamorphism in basement granitoids, Cooper Basin, South Australia

Andrew Y. Glikson^{1*} and I.Tonguç Uysal²

¹Australian National University

²Queensland Geothermal Energy Centre of Excellence, The University of Queensland

*Corresponding author: Andrew.Glikson@anu.edu.au

The original observation of parallel closely spaced (microns to tens of microns) planar features in quartz grains from basement granitoid samples of Cooper Basin drill holes by I.T. Uysal, followed by Universal stage, scanning electron microscope (SEM) and energy dispersive spectrometry (EDS) tests by A.Y. Glikson, identify intracrystalline planar deformation features (PDF) in quartz which correspond to unique Miller indices diagnostic of shock metamorphism. U-Stage measurements of angles between the C-optic axis of quartz (C_{qz}) and poles to planar deformation features (P_{pdf}) in the same quartz grains (87 planar sets in quartz 54 grains) define intracrystalline planar orientations dominated by $\{10\bar{1}3\}$ and $\{10\bar{1}2\}$ Miller indices, correlated with shock pressures above 10 Gpa and above 20 Gpa, respectively (Engelhard and Stoffler, 1968; French, 1968; Stoffler, 1974; Stoffler and Langenhorst, 1994; Grieve et al., 1996; French, 1998). These Miller indices are characteristic of large impact structures, including Chesapeake Bay (D~85 km), Woodleigh (D~120 km) and other impact structures. SEM/EDS studies of core samples indicate features consistent with shock metamorphism, including recrystallized pseudotachylite veins and microbreccia veins injected into resorbed quartz grains. Extensive alteration of feldspar to sericite and illite represent hydrothermal effects. Negative Bouguer anomalies of c. $-20 \mu\text{m/s}^2$ below parts of the Cooper Basin reflect low density basement sectors ($2.64\text{-}2.76 \text{ gr/cm}^3$) as compared to adjacent high density basement terrains ($2.9\text{-}2.99 \text{ gr/cm}^3$), consistent with impact fracturing of target rocks. Low magnetic anomalies of c. -200 nT associated with the Moomba structural dome and similar structures to the northeast may represent reset magnetisation such as is commonly associated with impact structures. An extension of the

Bouguer and magnetic anomalies over a >80 km-long belt defines the minimum extent of the shock metamorphosed basement, consistent with measured shock pressures of above 20 GPa. A regional altered zone at the top of the basement approximately $10,000 \text{ km}^2$ large and up to 524 meters deep (Boucher, 2001) may correspond to the impact aureole. Domal seismic structural elements and overlying unconformities in overlying sedimentary sequence of the Cooper Basin may be related to post-impact isostatic uplift of impact-fractured low-density basement sectors. The evidence for impact bears potential implications for the origin of K-U-Th enrichment in the basement in terms of an impact-triggered hydrothermal cell, mobilization and reconcentration of radiogenic elements.

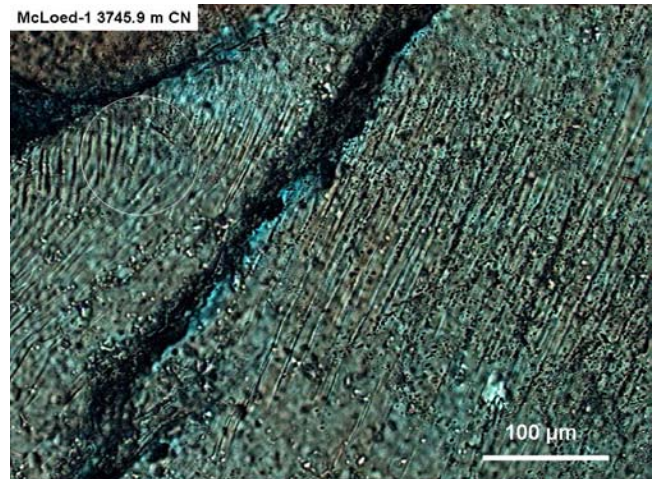


Fig. 1. Planar deformation features (PDF) in quartz deflected along a post-impact fracture, McLoed-1 3745 m.

Identification of planar deformation features (PDF)

Penetrative intracrystalline planar deformation features (PDF) in quartz possess specific crystallographic Miller indices with orientations diagnostic of shock metamorphism at pressures in excess of levels associated with endogenic processes such as seismic shock, volcanic explosions and shear processes which produce metamorphic deformation lamella (MDL) in quartz (Engelhard and Stoffler, 1968; French, 1968; Stoffler, 1974; Stoffler and Langenhorst, 1994; Grieve et al., 1996; French, 1998; French and Koeberl, 2010) (Figs 1 - 5). PDFs are (1) restricted to individual grains, i.e. they do not cross grain boundaries; (2) are often multiple, with N sets per grain; (3) have a strict planar character though they can be deflected along shear zones and fractures and in some instances fan out; (4) are typically 2-4 micron wide; (5) are closely spaced, typically 10-20 micron; (6) consist of glassy or recrystallized quartz mosaic lamellae, or are marked by arrays of fluid inclusions; (7) possess unique crystallographic orientations.

Shock metamorphic features are classified in the following terms (French, 1998):

1. Mineral fracturing {0001} and {10⁻¹¹} in quartz: 5-7 GPa
2. Basal Brazil twins {0001}: 8-10 GPa
3. PDF in quartz {10⁻¹³}: >10 GPa
4. Transformation of quartz to stishovite: 12-15 GPa
5. PDF in quartz {10⁻¹²}: >20 GPa
6. Transformation of quartz to coesite - >30 GPa

The results of universal stage measurements are presented in Figs 4 and 5. U-stage analysis of PDF orientations is complicated by a number of factors, arising from differential deformation related to the attenuation of shock of quartz grains by enveloping hydrous phases, as well as post-shock deformation (Figs 1, 2) and recrystallization of quartz grains). This includes superposition of multiple sets of planar features, including well defined parallel micron-scale to tens of micron-scale PDF sets (Fig. 3) and less well-defined to poorly defined parallel or undulating planar features, including deformed PDF and planar features (PF) formed by pre-impact and/or post-impact deformation (Figs 1, 2). By contrast to PDFs planar features may show degrees of undulation and waviness and may be accompanied by fluid inclusions and cryptocrystalline clouding (Fig. 3). Rarely are PDFs completely expressed and a high proportion of grains display only one or two PDFs.

Planar features displayed by quartz grains of the Moomba-1 and McLoed-1 samples include genuine PDFs defined by:

1. Penetrative planar parallel sets with spacings on the scale of few microns to few tens of microns (Figs 1 - 3).
2. Differential development of PDFs between grains and within grains.
3. Common association of PDFs with less-well defined inclusion-marked somewhat curved fracture sets (Fig. 3).
4. Post-impact deformation indicated by drag-fold features along younger microfractures (Fig. 1) and wavy deformation of PDFs within grains (Fig. 2).

In the present study PDFs were measured on planar sets displaying high degree of parallel orientation at a few microns to few tens of micron intervals. PDFs measured in quartz grains of the Moomba-1 and McLoed-1 samples are plotted in Figs 4 and 5 in terms of percent frequency of PDFs which correspond within measurement accuracy of $\pm 3^\circ$ to specific Miller indices of {10⁻¹³}, {10⁻¹²}, {11⁻²²}, {11⁻²¹}, {10⁻¹¹} and {51⁻⁶¹}.

The plots demonstrate a prevalence of PDFs with Miller indices of {10⁻¹³} and {10⁻¹²} in Moomba-1 core samples and of Miller index of {10⁻¹²} in the McLoed-1 core samples (Figs 4, 5), suggesting shock pressures of >20 GPa in both cores in accord with criteria indicated in studies of shock deformation of quartz (Engelhard and Stoffler, 1968; French, 1968; Robertson et al., 1968; Stoffler, 1974; Stoffler and Langenhorst, 1994; Grieve et al., 1996; French, 1998; French and Koeberl, 2010). Other measured Miller indices diagnostic of shock metamorphic effects include {11⁻²¹}, {11⁻²²}, {10⁻¹⁰}, {10⁻¹¹} and {51⁻⁶¹}.

PDF indices correlated with shock pressures of >20 GPa are found in large to very large impact structures, including Yarrabubba impact structure, Western Australia (Macdonald et al., 2003), Woodleigh impact structure, Western Australia (D=120 km; age ~359 Ma) (Glikson et al., 2005A, B), Chesapeake Bay impact structure (D=85 km; age ~35 Ma) and large Canadian impact structures (Type D) (French and Koeberl, 2010).

Moomba-1 2857.4 m PPL

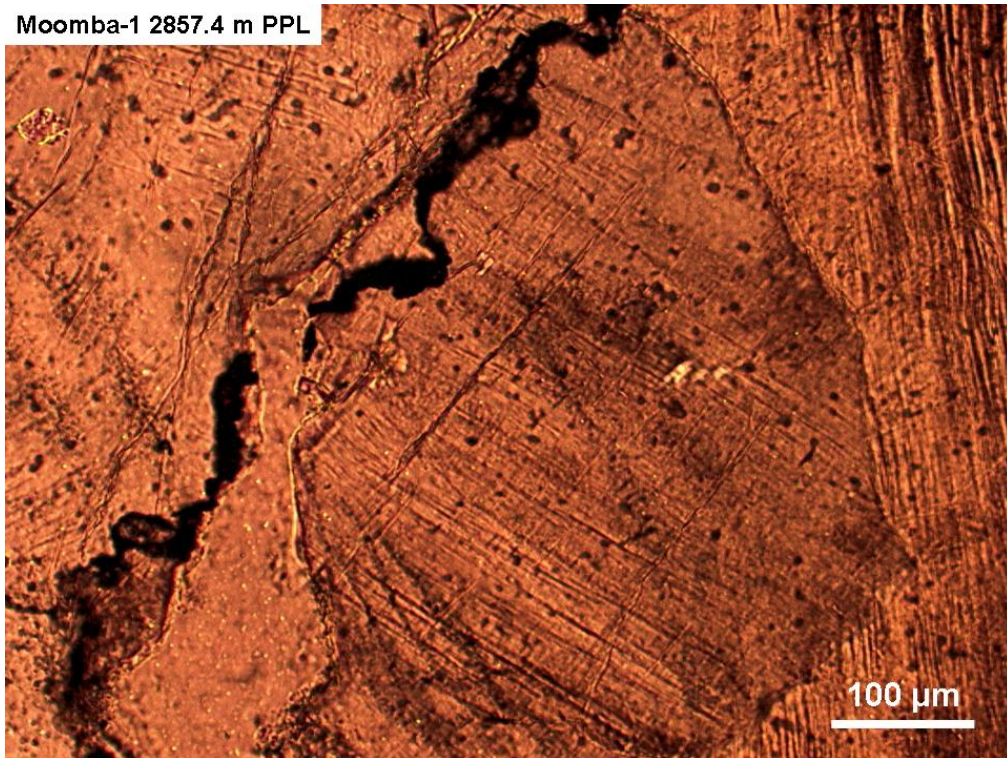


Fig. 2. Three quartz grains bearing planar deformation features (PDF): Note the wavy planar structure of the right-hand grain, representing post-impact plastic deformation of the quartz grain. Moomba-1 2857.4 m PPL.

Moomba-1 2857.4 m CN

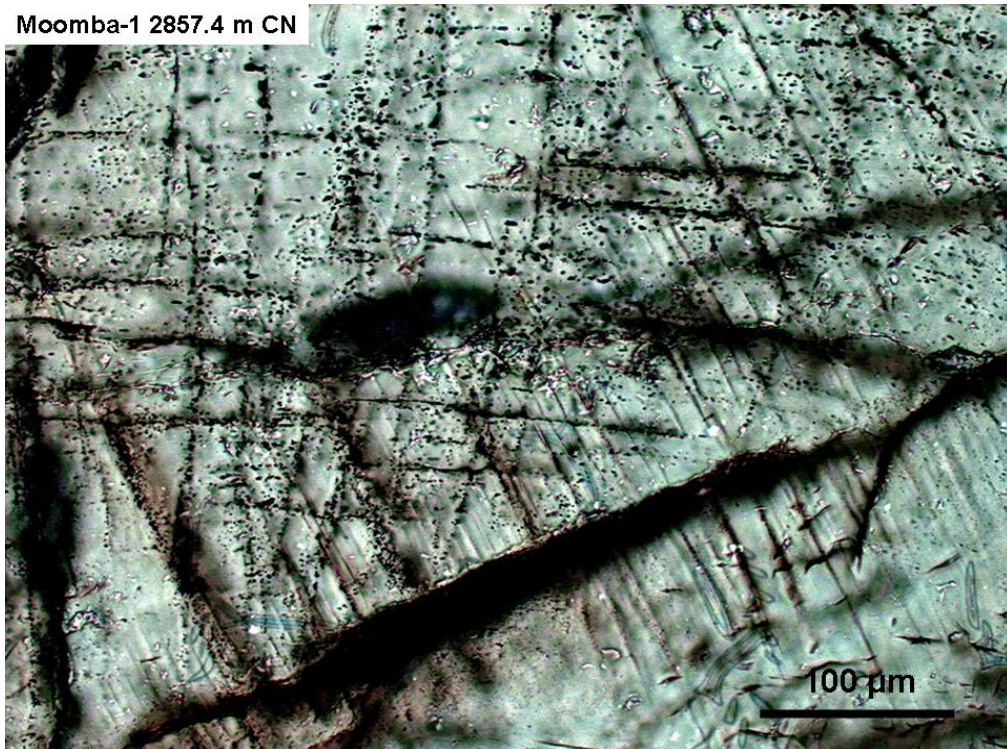


Fig. 3. Planar deformation features (PDF) (NNW-trending at lower and right-hand part of image) and inclusion-dotted planar fractures (at left side of image). Moomba-1 2857.4 m, PPL.

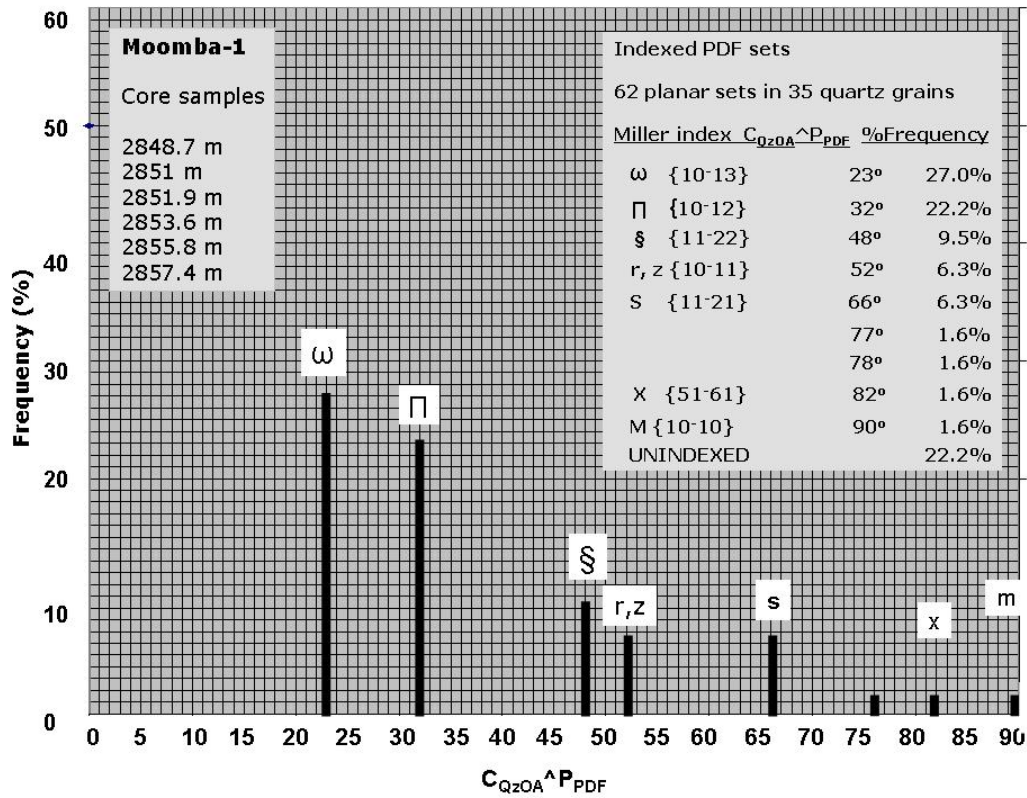


Fig. 4. Percent frequency distribution of the Miller-indexed angles between C-optic axis of quartz grains (C_{QzOA}) and the pole to planar deformation features (P_{PDF}) in 62 planar sets in 35 quartz grains from Moomba-1 granitoid core samples. Planes are indexed within measurement accuracy of $\pm 3\%$ of Miller indices.

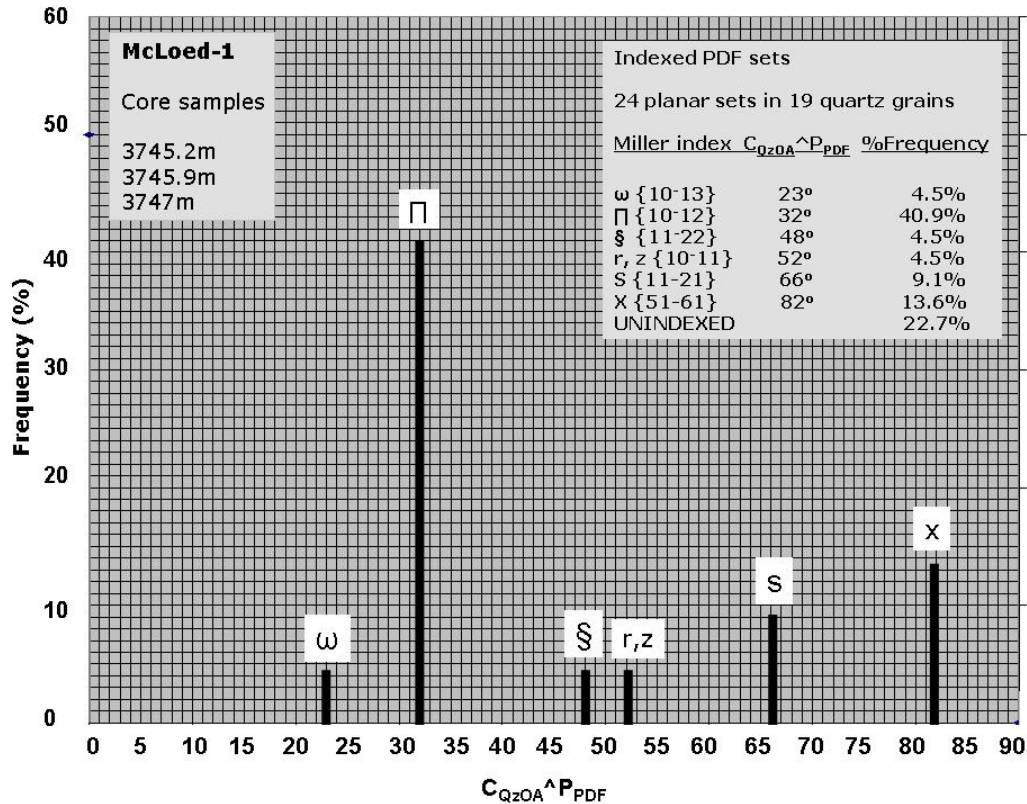


Fig. 5. Percent frequency distribution of Miller-indexed angles between C-optic axis of quartz grains (C_{QzOA}) and the pole to planar deformation features (P_{PDF}) in 24 planar sets in 19 quartz grains from McLoed-1 granitoid core samples. Planes are indexed within measurement accuracy of $\pm 3\%$ of Miller indices.

Scanning electron microscopy and energy dispersive spectrometry

Three samples were analysed by scanning electron microscopy (SEM) and Energy Dispersive Spectrometry (EDS) on a Jeol-6400 electron microscope at the Research School of Biological Studies, Australian National University (analyst: A. Glikson; supervisors: F. Brink, H. Chen). SEM/EDS analytical procedures included point analyses of element abundances at detection levels of >2000 ppm. Using a 15 KeV accelerating voltage, spot analyses were carried with a 1 micron-size beam, with a spectrum collection time of 80 seconds (120 seconds real time) at 8000 cps. Accuracy and precision are based on reference standards by Astimex Scientific Limited MINM25-53 (Serial Number 95-050) using standard olivine, diopside, almandine garnet, albite and barite.

Studied samples include:

Moomba-1 2857.4 m (Fig. 6): Altered coarse-grained granitoid consisting of quartz with resorbed grained boundaries injected by microbreccia veins which consist of micron to tens of micro-scale quartz, sericite/illite, sulphide and minor magnetite.

McLoed-1 3745.9 m: Altered coarse-grained granitoid containing K-feldspar, albite and sericite/illite, injected by microbreccia veins. Hydrothermal alteration is manifested by partly corroded/resorbed quartz grains and magnetite grains.

Big Lake-1 3057m: K-feldspar-albite-quartz granitoid consisting of resorbed quartz fragments injected by microbreccia.

EDS analyses indicate an abundance of sericite and occasional preservation of K-feldspar and albite. Observations relevant to the search for shock metamorphic features include:

1. Planar deformation features identified by optical microscopy do not display on either electron backscatter mode or secondary electron (SE1) scanning mode. This indicates PDF lamina consist of cryptocrystalline quartz of similar electron density as the host quartz.
2. The injection of microbreccia veins into quartz grains is consistent with, although does not prove, shock effects.
3. The corroded boundaries of quartz and magnetite grains (Fig. 6) and the abundance of sericite and illite are consistent with hydrothermal alteration of the granitoids.

The extreme fine grained texture of the microbreccia veins suggests their possible derivation by recrystallization of pseudotachylite veins consisting of impact-generated comminuted and fluidized material similar to veins found around exposed impact structures (Spray, 1995; Spray and Thompson, 1995; Reimold, 1995, 1998).

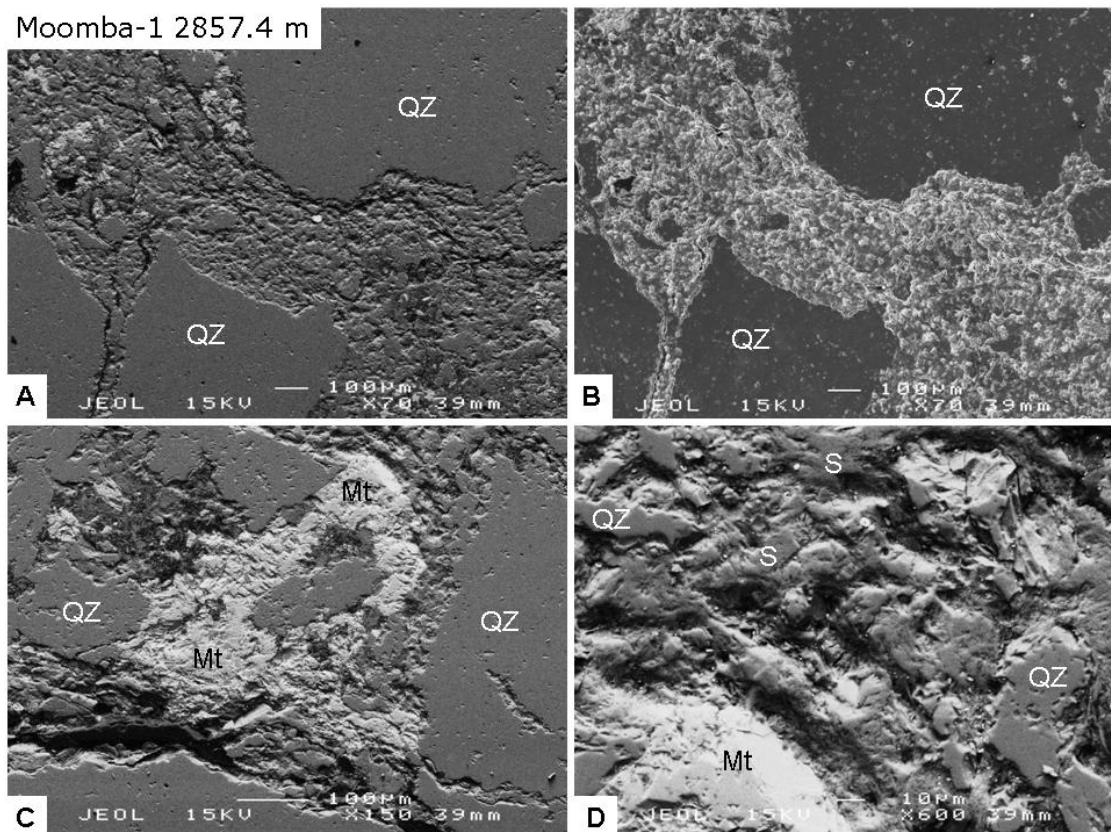


Fig. 6. Moomba-1 2857.4 m: SEM image of hydrothermally altered microbreccia-injected granitoid. (A) backscatter image of microbreccia veins injected into quartz grains; (B) SEI image of frame A; (C) secondary magnetite within microbreccia veins; (D) magnified view of microbreccia vein consisting of quartz, sericite and magnetite.

Implications for structure and the origin of geothermal anomalies

Boucher (1996, 2001), on the basis of wireline log signatures and drill cores, reported an altered zone up to 524 meters-thick at the top of the top of early to mid Palaeozoic basement underlying the Cooper Basin. Boucher (2001) considered the origin of this zone in terms of either weathering or hydrothermal alteration, or merely as a wireline logging anomaly.

The presence of signatures of shock metamorphism within the altered top basement zone may suggest extensive hydrothermal activity triggered by a large asteroid impact, as has been documented in large impact structures (Allen et al., 1982; Naumov, 2002; Pirajno, 2005; Glikson et al., 2005; French, 1998; Uysal et al., 2001, 2002; French and Koeberl, 2010). Based on association of hydrothermal alteration with impact effects, the extent of the impact aureole may be outlined by the altered zone, which covers an area larger than 10,000 km² in the Cooper Basin (Boucher, 2001; Fig. A8).

Shock metamorphism of basement sectors is consistent with geophysical and structural evidence for low density (2.64–2.76 g/cm³) basement sectors underlying the Moomba-1 and McLoed-1 holes, as compared to higher density bodies (2.8 – 3.0 g/cm³) in adjacent terrain (Meixner et al., 2000). The low-density basement sectors likely represents intense hydration and fracturing related to the impact, as is the case with the Woodleigh impact structure (Glikson et al., 2005a, 2005b), Gnargoo probable impact structure (Iasky and Glikson, 2005) and Mount Ashmore probable impact structure (Glikson et al., 2010). The low magnetic anomalies associated with the gravity lows (Meixner et al, 2000) are consistent with demagnetisation of impacted basement zones, observed in a number of impact structures (Grieve and Pilkington, 1996).

The evidence for impact bears potential implications for the origin of K-U-Th enrichment in the Cooper Basin in terms of an impact-triggered hydrothermal cell and associated mobilization and reconcentration of radiogenic elements. Temperatures over 225°C at 5 km depth (T_{5km}) occur over an area about 79,000 km² large under an insulating sedimentary cover about 3.5 – 4.5 km-thick at the Nappamerri Trough between Moomba dome and Innamincka where geothermal gradients as high as 55-60°C/km are measured (Middleton, 1979; Wyborn et al., 2004;

Radke, 2009). The highest temperatures occur near Innamincka in the proximity of McLoed-1, where maximum shock pressures of >20 Gpa are measured (Fig. 5). Extreme total heat flow of 7.5-10.3 mWm⁻³ originate from enrichment of the Big Lake Suite granites in radiogenic heat-producing elements, including Uranium (13.7, 16.5 ppm), Thorium (46, 74 ppm) and Potassium (5.2, 6.0% K₂O) (Middleton, 1979; Sandiford and McLaren, 2002; Chopra, 2003; McLaren and Dunlap, 2006). The presence of a highly radiogenic basement within 3-4 km of the surface may in part reflect upward migration and re-concentration of large ion lithophile elements associated with an impact-generated hydrothermal cell, as is the case in some impact structures, including Woodleigh (Glikson et al. 2005), Shoemaker impact structure and Yarrabubba impact structure (Pirajno, 2005).

References

- Allen, C. C., Gooding, J. L., Keil, K. 1982. *Journal of Geophysical Research* **82**, 10083 – 10101.
- Boucher, R.K., 1996. MESA Journal, 21, 30-32.
- Boucher, R.K., 2001. Nature and origin of the altered zone at the base Cooper Basin unconformity, South Australia. *South Australia. Department of Primary Industries and Resources, Report Book 2001/012*.
- Chopra, P., 2003. *Preview Australian Society of Exploration Geophysics*, **107**, 34-36.
- Engelhard, W.V., Stöffler, D., 1968. in: *Shock Metamorphism of Natural Materials*. Mono Book Corp, Baltimore, MD, 159-168.
- French, B.M., 1968. In: *Shock Metamorphism of Natural Materials*. Mono Book Corp, Baltimore, MD, 1-17.
- French, B.M., 1998. Traces of catastrophe: a handbook of shock-metamorphic effects in terrestrial meteorite impact craters. *Lunar and Planetary Institute, Houston, TX, Contribution CB-954*. 120 pp.
- French, B.M., Koeberl, C., 2010. The convincing identification of terrestrial meteorite impact structures: What works, what doesn't, and why. *Earth-Science Reviews*, **98**, 123-170.
- Glikson, A. Y., Eggins, S., Golding, S., Haines, P. W., Iasky, R. P., Mernagh, T. P., Mory, A. J., Pirajno, F. Uysal, I. T., 2005. *Australian Journal of Earth Sciences*, **52**, 555-573.
- Glikson, A. Y., Mory, A. J., Iasky, R. P., Pirajno, F., Golding, S. D., Uysal, I. T. 2005. *Australian Journal of Earth Sciences*, **52**, 545-553.
- Glikson, A. Y., Jablonsky, D., Westlake, S., 2010. *Australian Journal of Earth Sciences*, **57**, 411-430.
- Grieve, R.A.F., Pilkington, M., 1996. *Australian Geological Survey Organisation Journal of Australian Geology and Geophysics*, **16**, No. 4, 399-420.
- Grieve, R.A.F., Langenhorst, F., Stöffler, D., 1996. *Meteoritics and Planetary Science*, **31**, 6-35.
- Iasky, R. P., Glikson, A. Y. 2005. *Australian Journal of Earth Sciences*, **52**. 575-586
- Macdonald, F.A., Bunting, J.A., Cina, S., 2003. *Earth and Planetary Science Letters*, **213**, 235-247
- McLaren, S., Dunlap, W.J., 2006. *Basin Research*, **18**, 189-203.
- Meixner, T.J., Gunn, P.J., Boucher, R.K., Yeats, A.N., Murray, L., Yeats, T.N., Richardson, L.M., Freares, R.A., 2000. *South Australia Exploration Geophysics*, **31**, 024-032
- Middleton, M.F. (1979) *Bulletin of the Australian Society of Exploration Geophysics*.
- Naumov, M. V. 2002. In: *Impacts in Precambrian Shields*, pp. 117 – 173. Springer Verlag, Berlin.
- Pirajno, F., 2005. *Australian Journal Earth Science*, **52**, 4/5, 587-606.
- Radke, B., 2009. *Geoscience Australia Record* 2009/25.
- Reimold, W.U., 1995. *Earth Science Reviews*, **39**, 247-265.
- Reimold, W.U., 1998. *Earth Science Reviews*, **43**, 45-47.
- Robertson, P.B., Dence, M.R., Vos, M.A., 1968. *Shock Metamorphism of Natural Materials*. Mono Book Corp, Baltimore, MD, pp. 433-452.
- Sandiford, M., McLaren, S., 2002. *Earth Planetary Science Letters*, **204**, 133-150.
- Spray, J.S., 1995. *Geology*, **23**, 1119-1122.
- Spray, J.G., Thompson, L.M., 1995. *Nature*, **373**, 130-132.
- Stoffler, D., 1974. *Fortschritte der Mineralogie*, **51**, 256-289.
- Stoffler, D., Langenhorst, F., 1994. *Meteoritics*, **29**, 155-181.
- Uysal, T., Golding, S. D., Glikson A. Y., Mory A. J., Glikson, M., 2001. *Earth and Planetary Science Letters*, **192**, 281 – 289.
- Uysal, T., Golding, S. D., Glikson, A. Y., Mory, A. J., Glikson, M., Iasky, R. P., Pirajno, 2002. *Earth and Planetary Science Letters*, **201**, 253-260.
- Wyborn, D., de Graaf, L., Davidson, S. and Hann, S., 2004. *Eastern Australian Basins Symposium II, PESA Special Publication*, 423-430.